Clays and Clay Minerals, Vol. 40, No. 1, 40–52, 1992.

CHARACTERIZATION OF THE END OF SMECTITE-TO-ILLITE TRANSFORMATION: DECOMPOSITION OF X-RAY PATTERNS

BRUNO LANSON[1]

Département de géologie, Ecole Normale Supérieure, 24 rue Lhomond
75231 Paris Cedex 05, France

GÉRARD BESSON

Centre de recherche sur la matière divisée, Rue de Chartres, B.P. 6759
45067 Orleans Cedex 2, France

Abstract—Complex X-ray diffraction (XRD) profiles are described crystallographically by simulating XRD peaks for each phase, and adding the various elementary patterns to fit the experimental X-ray pattern. X-ray patterns of a ground muscovite and three polyphasic diagenetic I/S samples are fitted with this powerful, but time-consuming, technique. In the 6°–10°2θ CuKα range, the asymmetry of the muscovite peak is related to a very broad coherent scattering domain size (CSDS) distribution; for the I/S samples the even greater asymmetry is due to the presence of several phases with close, but distinct crystallographic characteristics (I/S, illite, and detrital mica).

A simulation-decomposition approach for modelling XRD patterns is introduced to describe quickly and accurately the various clay minerals (essentially mixed-layer illite/smectite and illite) present in a sedimentary series, and to follow their individual evolution during diagenesis. The theory for these simulations is described briefly. The influence of mixed-layer heterogeneity (the distribution of CSDS, and the distribution of smectite content) on the shape of X-ray peaks is shown theoretically to be minimal. Indeed, for both CSDS and smectite content, the important parameter for peak shape appears to be the mean value of the distribution and not its width and/or its shape. The theoretical limitations of the decomposition method are presented. Minor experimental limitations (reproducibility, experimental peak shape, discrimination) make this method a powerful and reliable tool to describe X-ray patterns. The method is used to show the simultaneous occurrence of three "illitic" phases in a sedimentary series from the Paris Basin. The respective evolution of the three phases is clearly evidenced by using this decomposition method. However, the precise identification of these different phases remains difficult to determine because of the difference in peak width between simulated and experimental X-ray patterns.

Key Words—Decomposition, Diagenesis, Illite, Illite/Smectite, Mixed-layer, Simulation, Smectite, X-ray diffraction.

INTRODUCTION

For over twenty years, the smectite-to-illite diagenetic transformation has been described extensively by many authors (Burst, 1969; Perry and Hower, 1970; Hower *et al.*, 1976; Boles and Franks, 1979; Środoń, 1979, 1984a; Velde *et al.*, 1986; Glasmann *et al.*, 1989; among many others). X-ray diffraction (XRD) has been the essential tool used to reveal an evolution that is characterized by the sequence: Smectite → random mixed-layer illite/smectite (I/S) → ordered mixed-layer I/S → Illite.

When the lithology is constant, there is a continuous decrease in the smectite content of each of the illite/smectite interstratified minerals with increasing depth, and thus with pressure-temperature conditions. Comparing the evolution of I/S in various sedimentary basins (Lahann, 1980; Środoń and Eberl, 1984; Velde, 1985; Velde *et al.*, 1986; Jennings and Thompson, 1986; Freed and Peacor, 1989) it is obvious that there is an important kinetic effect in this transformation. This effect is seen also when comparing both the evolution of clay minerals and the maturation of organic material (Velde and Espitalié, 1989).

In order to characterize and model the kinetics of this reaction, it is essential to determine the reaction mechanisms. To describe these mechanisms, one must characterize, as accurately as possible, the various clay phases* existing in the sediment. In most of the diagenetic series, this identification is complex because of the simultaneous presence of several phases (I/S mixed-layer phases) with distinct, but closely-related crystallographic characteristics.

To identify these phases precisely using XRD, one must simulate separately each of these phases and then add the simulated patterns to fit the experimental data. Such simulations have been done by Besson (1980) and Ben Hadj-Amara *et al.* (1987) on monophasic smectite samples, and by Sakharov and Drits (1973), Reynolds (1980), Środoń (1980, 1984b), Inoue *et al.*

[1] Present address: U.S. Geological Survey, Box 25046, Mail Stop 404, Federal Center, Denver, Colorado 80302.

(1990), and Tchoubar *et al.* (1990) on mixed-layer minerals. But, this powerful method is so time-consuming that its routine application on dozens of samples is difficult.

Several authors (Środoń, 1979, 1980, 1981, 1984b; Watanabe, 1981, 1988; Velde *et al.*, 1986) have proposed alternative methods allowing a "quick" identification of a great number of samples. These methods are mainly based on peak position in simulated XRD patterns. However, X-ray patterns observed in a diagenetic series show several major characteristics that render identification difficult. Most often, in the angular range from 2°–10°2θ CuKα, which contains most information on CSDS (Reynolds and Hower, 1970; Środoń, 1980), the partial overlapping of characteristic peaks of chlorite, interstratified phases, illite, and/or detrital mica makes it difficult to separate the different contributions to the XRD peaks. However, separation of diffraction effects is essential for most of the classical I/S identification methods (Watanabe, 1981, 1988; Środoń, 1979; Velde *et al.*, 1986). The other methods require measurements on higher-angle peaks (Środoń, 1980, 1981, 1984b). These measurements are difficult to do routinely because of the low intensity of these peaks, and because of frequent overlapping with other phases (e.g., peak 002 with chlorites, peak 003 with quartz, all 001 peaks with detrital mica).

The problem of overlapping XRD peaks exists over the whole angular range. The complex peak located between 4° and 10°2θ CuKα appears to be the most interesting: 1) because of its high intensity; 2) because of the presence of all the illitic phases and only these phases; 3) and because of the availability of some critical information (e.g., CSDS) in this domain. To describe this diffraction band it was necessary to create a program enabling the separation of the different contributions to the diffraction intensity from each clay phase. This decomposition program can fit the experimental XRD pattern with elementary curves that are related to the different phases present in the sediment. The position and full width at half maximum intensity (FWHM) of these elementary curves should let us identify each associated phase by comparison with simulated patterns.

We first demonstrate that it is possible, with a crystallographic approach, to model even complex polyphasic X-ray diffraction (XRD) profiles. Indeed, XRD patterns of some diagenetic multiphase samples are simulated using the results of Lanson and Champion (1991) about the number and the nature of illitic phases present in these samples. Then, the much faster simulation and decomposition method is developed. The influence of the sample heterogeneity (CSDS and smectite content distributions) on XRD profiles is checked theoretically, as well as the influence of the ordering type (partial and maximum orderings for R = 1). The peak symmetry hypothesis made while writing the decomposition program is checked. The influence of instrumental factors and sample preparation are tested, as well as sample representativity. The discrimination power of the decomposition technique is tested on a theoretical mixture, and both the influence of ethylene glycol saturation on a ground sample of muscovite (and thus the possible effect of interparticle diffraction), and the effect of cation (Sr) saturation on our samples (hydration state of these samples) are determined. Finally, experimental patterns obtained from the studied diagenetic series are decomposed. It is possible to describe the diagenetic evolution of each phase considered separately, and to characterize all of these phases in order to define the reaction mechanisms controlling the diagenetic evolution of I/S mixed-layer clay. TEM observations and XRF analyses performed by Lanson and Champion (1991) gave us essential data on both the number and the chemistry of the different phases present in the samples.

EXPERIMENTAL

Samples

The samples studied are drill cuttings from a deep borehole C (2150 m) in the eastern Paris Basin near the town of Nancy (supplied by the Institut Français du Pétrole). Lanson and Champion (1991) described the stratigraphic sequence, and displayed some characteristic X-ray patterns from this borehole. Sixty-two samples from the drill hole were used to establish the general diagenetic trend in the I/S minerals. Lanson and Champion (1991) performed XRD analyses with numerical decomposition treatment, TEM morphological studies, XRF chemical analyses, and energy dispersive spectroscopy (EDS) on individual particles to characterize four of these samples and to show the I/S transition stages. The essential criterion for the selection of these samples (from 1000, 1550, 1730, 2130 m depth) was the absence, or the very low abundance, of other phases such as chlorite, kaolinite, or carbonates to avoid confusion for TEM observations. The different origins of the sediments could have had an influence on their diagenetic evolution. The great consistency observed in the evolution of these sediments (Lanson and Champion, 1991; see below) indicates that this influence was only minor, if it exists at all.

Several other samples were chosen, due to availability and similarities in I/S smectite content, to test the reproducibility of the method and to test the va-

* In this paper, the word "phase" describes a population of particles whose physico-chemical composition vary about a mean value. It is assumed that this population behaves as a monophasic material (in a thermodynamic sense) having the same mean characteristics. Consequently this word is also used in the thermodynamic sense throughout the paper for this material.

lidity of the description of a stage of diagenetic evolution with one representative sample. Eleven samples from the same Jurassic outcrop, near Lons le Saunier in the French Jura, were used to test the variability on the scale of a meter-size outcrop. Five different stratigraphic levels (Barremian, 850–950 m, to Kimmeridgian, 1250–1400 m) were sampled in seven neighboring deep wells located in the Meaux area, east-central Paris Basin. It is important to note that because these wells are located in the same area, sampling depths for the same stratigraphic level are almost the same in these different wells. Thus, the diagenetic evolution of these samples not only results from their common origin, but also, and mostly, from their similar thermal history. A ground muscovite sample from Northern Scotland, used as a standard for the X-ray diffractometer, also was used to check the influence of ethylene glycol saturation on pure mica particles.

Experimental methods

The <2-μm fraction was separated and brought into suspension in distilled water. After 24 hours of sedimentation, the upper six centimeters of the suspension were extracted. This fraction was passed through a Millipore filter (0.4 μm) in order to concentrate the material, and to get an optimum orientation (Reynolds, 1986). Samples were run on a Philips PW1050/20 diffractometer with a stepping motor drive on the goniometer. Ni-filtered CuKα_1, Kα_2 radiation (fine-focus tube; Philips PW2213/20) was used. Motor and intensity acquisition (Siemens proportional detector) commands were effected using a Socabim DACO system. Divergence slit, receiving slit, and scatter slit were respectively 1°, 0.1 mm and 1°. Ethylene glycol saturation was performed using liquid ethylene glycol and a small brush. The excess ethylene glycol was removed by pressing the slide on an absorbant paper. Usual step size and counting times were respectively, 0.01°2θ and 3 seconds for air-dried (AD) patterns and 4 seconds for ethylene glycol-saturated (EG) patterns. If necessary, greater counting times were used to obtain a better spectrum. Usually, no particular exchangeable cation was used. For some typical samples, patterns of Sr-saturated and untreated samples were compared. No differences were found (see below).

Simulation of X-ray diffraction patterns

Various mathematical expressions for X-ray diffraction intensity have been published (Mering, 1949; Hendricks and Teller, 1942; Drits and Sakharov, 1976; Tchoubar *et al.*, 1990). To simulate mixed-layer X-ray patterns, it is necessary to define on the one hand the different elementary interstratified layers and, on the other hand, the stacking sequence in each crystallite, defined by the junction probabilities of elementary layers. The structure of the different elementary layers, as well as the junction probabilities used for this work, are detailed by Lanson (1990). All the simulations were calculated with the CALC program created at the University of Orleans, France. CALC allows very easy modifications of junction probabilities, and allows calculation of mixed-layer minerals with three components. For most calculations, this program and the NEWMOD program (Reynolds, 1985) gave equivalent results. However, when looking to the structure factors for different layer types, Lanson (1990) noted differences between the two programs. Structure factors obtained with CALC are similar to those determined by Drits and Sakharov (1976) and vary with layer type. On the other hand, structure factors calculated with NEWMOD are very similar, whatever the layer type is (illite, smectite-1H_2O, smectite-2H_2O, smectite-1EG, or smectite-2EG), because the NEWMOD program does not take into account the exchange cation, as well as the EG and/or water sheets located on the edges of the particles. Thus, one-layer illite and one-layer smectites (hydrated or glycolated) are identical when calculated by NEWMOD. This should be kept in mind, especially when assuming small CSDS, because it could induce major differences in the resulting calculated profiles.

We did not use long-range stacking junction probabilities (Reichweit $\geq$ 2), even for highly illitic material (% Sm $\leq$15). For such highly illitic material the X-ray pattern is mostly a function of the illite layer, which is the essential (quasi-exclusive) component. The patterns obtained for such illitic materials with long range ordering are quite similar to those obtained with short range, R = 1, as they show a similar trend either in a peak position–% smectite plot (Figures 5–8; Środoń 1980, Figure 7; Środoń 1984b) or in a $\Delta 2\theta_1$–$\Delta 2\theta_2$ diagram (Figure 5; Watanabe, 1988). This analogy allows us to identify the natural I/S mixed-layers with long-range ordering (R $\geq$ 2), if they do exist in diagenetic series, by comparison with short-range (R = 1) ordering simulations. Furthermore, in I/S mixed-layer clays the bonding between the different layers is mostly ionic. Thus, the influence of this bonding is less than or equal to a one-layer thickness. Thus, the occurrence of a given layer will depend only on its nearest neighbors and not on greater distance neighbors.

Influence of mixed-layer I/S heterogeneity on X-ray diffractogram shape. Clay minerals from a diagenetic environment are not unique and perfectly homogeneous materials. Indeed, these minerals result from the transformation of an initially heterogeneous material. This transformation involves several reactions that are controlled by reaction kinetics. Consequently, clay phases are particle populations with variable sizes (*ab* plane), thicknesses (along the c* axis), and compositions (smectite content, as well as chemical composition of individual layers).

For a hydrothermal series of illites, Inoue *et al.* (1988) proposed a transformation similar to Ostwald ripening. During such a transformation, thickness distributions are quite broad, and will change as smaller crystals dissolve and larger ones grow. According to Nadeau *et al.* (1984a, 1984b), mixed layering is related to an interparticle diffraction phenomenon; the apparent "smectite content" being determined by the number and the thickness of fundamental illite particles that are coherently stacked. In this latter case, the decrease "in smectite content" results from the increase of the thickness of these fundamental illite particles, and the CSDS varies as a function of sediment evolution. In both cases, simultaneously with the CSDS distribution there is also a composition (illite content) distribution induced either by the coexistence of particles with various amounts of smectite, induced by dissolution and growth in the first hypothesis, or by the relaxation of the structure inducing a change in composition on the edges of fundamental particles. This distribution of composition follows a Markovian law (Drits and Sakharov, 1976; Tchoubar *et al.*, 1990).

Lanson (1990) showed that the characteristics of simulated patterns depend essentially on the mean values of composition (illite content) and/or CSDS for a given particle population. The shape and width of the distribution for both of these parameters is much less influential. Thus, the composition and the CSDS determined by comparison of the experimental diagrams with simulated patterns should be considered as a mean value for heterogeneous populations that we are not able to describe accurately. The heterogeneity would exist not only for CSDS and/or composition (illite content), but also for internal layer composition (number, amount, and position of the different atoms in the structure), and for the stacking sequence. It is essential to keep this in mind, and not to consider the identified mixed-layer mineral as a unique homogeneous phase, but rather as the reflection of a population of particles that results from a kinetic growth process.

Decomposition method

To describe a complex X-ray pattern in the angular range from 4°–10°2θ CuKα it is necessary to decompose it, in order to separate the contributions of each phase present. For this decomposition program, symmetrical Lorentzian (Cauchy) and Gaussian shapes were selected. These functions have only a minimum of adjustable parameters (position, FWHM, and intensity), and the fits obtained with these two shapes were very satisfying (Lanson and Champion, 1991). Thus, we did not consider more complex functions with a greater number of parameters such as asymmetry factors.

This decomposition method is a multistep process. To decrease the effect of statistical counting errors, a preliminary smoothing is performed. To eliminate most of the contribution of the Lorentz-polarization factor, a "background" is subtracted from smoothed patterns. Finally, the elementary peak fit is performed either with a least squares method (Press *et al.*, 1986), or with a non-linear downhill simplex method (Nelder and Mead, 1965; Press *et al.*, 1986). The calculation algorithms used for X-ray pattern processing (smoothing, background stripping, and elementary peak fitting) are classical and have been detailed by Lanson (1990).

For pattern fitting, the number of elementary curves is set by the user, who should make very careful assumptions. For AD profiles, the recommended procedure is to progressively increase the number of curves in order to get a good fit with the smallest possible number of elementary peaks. If possible, the number of elementary peaks should be checked by direct observations of the sample (e.g., TEM). For EG profiles, the number of elementary peaks will be a function of both the number of phases found for the AD profile, and of the assumed nature of the associated phases (expandable or not), in order to obtain consistent results from both AD and EG profile decompositions (Lanson and Champion, 1991). For decomposition of the EG profile, there should be an elementary peak related to any elementary peak fitted on the AD profile. Furthermore, if this elementary peak is associated with an expandable I/S phase, an additional peak is to be introduced, because a doublet is associated with glycolated I/S mixed-layer phases in this angular range (one peak on each side of 10 Å).

The approximation of experimental profiles with symmetrical functions (Gaussian and/or Lorentzian) was found to be adequate. Usually the best fits were obtained assuming Gaussian shapes for any elementary peak containing both Kα1 and Kα2 radiations. However, Howard and Preston (1989) found this Gaussian profile inappropriate for routine X-ray diffraction work.

The decomposition method has to be used keeping in mind several approximations and limitations. To confirm the observations made on the basis of this method (e.g., one peak–one phase), one must verify that the theoretical pattern, which is the sum of all simulated patterns of phases identified in the sample, is similar to the experimental pattern over the whole angular range.

Direct TEM observations of the sample would also be useful to check the existence of the different phases identified with XRD, because the pattern decomposition has a physical meaning only if the modeled phases correspond to phases that actually exist in the sediment. In this case only the contributions of each phase are added, and it is then possible to decompose (or to desum) the experimental pattern.

In diagenesis, any of the "phases" related to these elementary curves is not formed from an unique homogeneous material, but represents a population of particles with variable physico-chemical characteristics. Any phase identified with this method will be

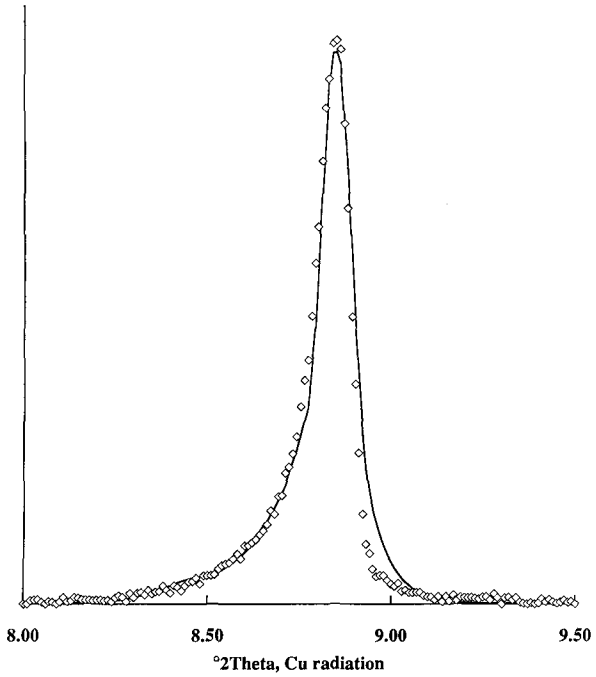

Figure 1. X-ray pattern of crushed muscovite used as a standard. Diamonds represent the experimental pattern; the solid line the calculated pattern. This pattern has been calculated fitting the proportions of five muscovite patterns (see text for composition) with different CSDS distributions (least squares method). This fit was done after background subtraction on both experimental and theoretical patterns.

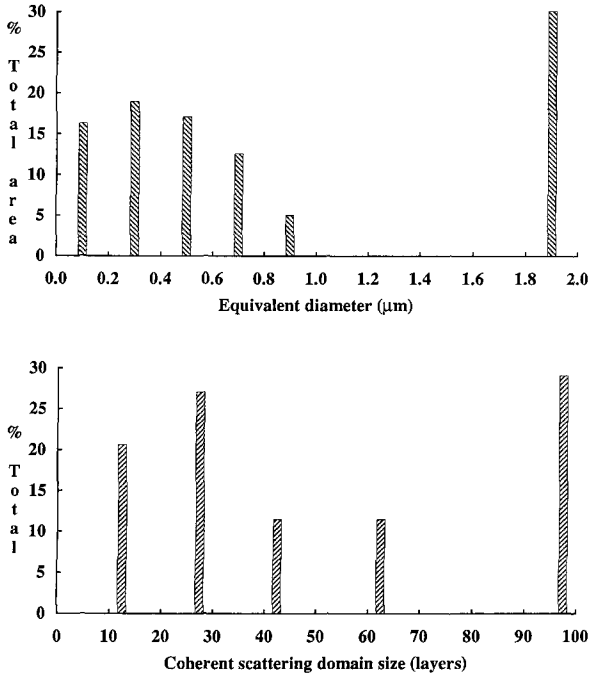

Figure 2. Comparison between equivalent diameter (Lanson and Champion, 1991) and CSDS distributions. The first distribution was obtained by TEM measurement of particle size. For each equivalent diameter class, the surface corresponding to all the particles of this class was calculated and divided by the total surface (sum of the surface for all the observed particles). The CSDS distribution was obtained fitting the proportions of five theoretical muscovite patterns on the experimental X-ray pattern (least squares method).

characterized by a mean value for all these parameters, with the mean values actually representing a population.

Furthermore, in the 4°–10°2θ CuKα range, the diffraction peak of any phase is asymmetric. Basically, one can consider that this results (Reynolds, 1980, 1989) from the product of the interference function (symmetrical) by the structure factor and the Lorentz-polarization factor (both strongly decreasing in this angular range). Thus, the decomposition of an experimental pattern using symmetrical elementary curves can be only an approximation.

EXPERIMENTAL RESULTS

X-ray pattern simulations

Natural crushed muscovite. This sample can be considered as a single phase. Thus, the asymmetry of the experimental pattern (Figure 1) can only result from the CSDS distribution (which includes defects; Reynolds, 1985). In order to verify this assumption, we summed patterns of muscovite (structural formula: $K^{+}_{1.00}(Fe^{3+}_{0.10},Mg^{2+}_{0.10},Al^{3+}_{1.80})$ $(Si_{3.10},Al_{0.90})O_{10}(OH)_2$) with CSDS varying between 5 and 100 layers. The 19 simulated patterns were separated into five groups as a function of their CSDS distribution: Group 1: [6,9], [11,14], [16,19]; Group 2: [21,24], [26,29], [31,34], [36,39]; Group 3: [41,44], [46,49], [51,54], [56,59]; Group 4: [61,64], [66,69], [71,74], [76,79]; and Group 5: [81,84], [86,89], [91,94], [96,99].

The sums were done with one pattern from each group to obtain the optimal fit shown on Figure 1. The relative proportions of each pattern were adjusted by the least squares method. According to Nadeau (1985), the CSDS of an I/S clay phase is related to its particle size. Thus, to check the consistency of this simulation, particles edges were digitized on TEM micrographs and the area and the equivalent diameter (diameter of the circle having the same area as the observed particle, Lanson and Champion, 1991) were determined for any particle. For each class of equivalent diameter it was possible to calculate the total surface of the particles of this class, and the relative proportion of this area over the global area for all the particles. This proportion is directly related to the contribution of this class of particles to the X-ray pattern of the sample.

As shown on Figure 2, the distributions of relative surface area versus equivalent diameter and versus the distribution of CSDS are similar in shape. The validity of the simulation is also shown by the good correlation between equivalent diameter and thickness of the particles (Figure 3). The relative proportions of the patterns added to obtain the fit shown in Figure 1 represent

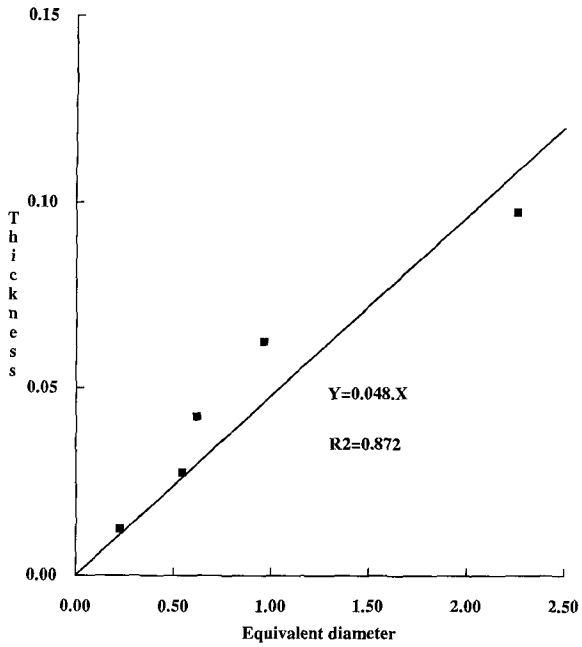

Figure 3. Correlation between equivalent diameter of the particles and their thickness: crushed, standard muscovite example. Values are given in micrometers. The linear regression was calculated with a 0 Y-value at the origin. Determination of couples (equivalent diameter, thickness) is explained in the text.

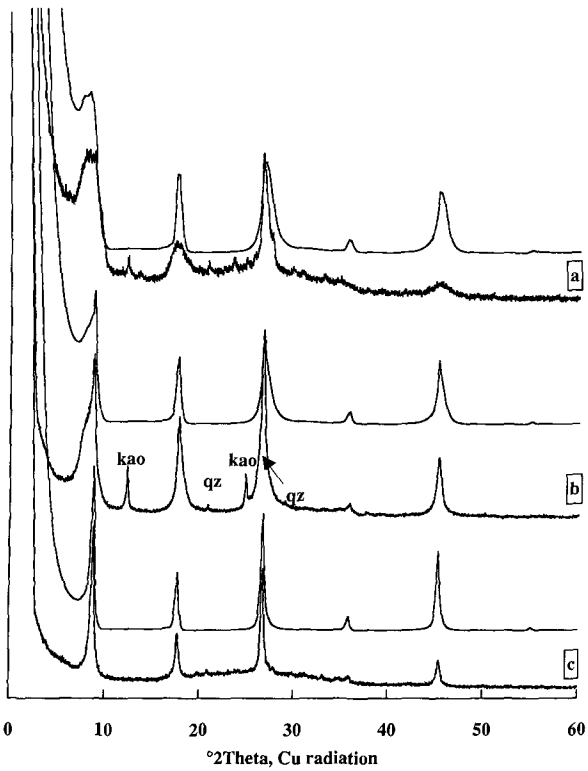

Figure 4. Comparison between experimental and simulated X-ray patterns. (a) AD pattern of C1000. Bottom: experimental pattern; top: theoretical pattern. The theoretical pattern is the sum of following elementary patterns: I/S 86% Ill, R 1 maximum ordering, $3 \leq N \leq 16$ (asymmetric distribution): 60%; I/S 94% Ill, R 1 maximum ordering, $7 \leq N \leq 16$ (asymmetric distribution): 34%; Mica 100% Ill, R 1 maximum ordering, $15 \leq N \leq 85$ (asymmetric distribution): 6%. (b) AD pattern of C1475. Bottom: experimental pattern; top: theoretical pattern. The theoretical pattern is the sum of following elementary patterns: I/S 88% Ill, R 1 maximum ordering, $3 \leq N \leq 16$ (asymmetric distribution): 44%; I/S 94% Ill, R 1 maximum ordering, $11 \leq N \leq 20$ (asymmetric distribution): 30%; Mica 100% Ill, R 1 maximum ordering, $15 \leq N \leq 85$ (asymmetric distribution): 26%. (c) AD pattern of C2130. Bottom: experimental pattern; top: theoretical pattern. The theoretical pattern is the sum of following elementary patterns: I/S 92% Ill, R 1 maximum ordering, $7 \leq N \leq 16$ (asymmetric distribution): 14%; I/S 98% Ill, R 1 maximum ordering, $11 \leq N \leq 20$ (asymmetric distribution): 48%; Mica 100% Ill, R 1 maximum ordering, $15 \leq N \leq 85$ (asymmetric distribution): 38%.

the relative amounts of material corresponding to particles with increasing CSDS. The CSDS values come from the assumptions used to simulate the theoretical muscovite patterns fitted on the experimental profile. The associated values of equivalent diameter (*ab*-dimension) were determined from the cumulative distribution of surface area as a function of equivalent diameter. The equivalent diameter corresponding to a certain CSDS is characterized by a similar proportion of material involved; proportion of the considered pattern on the one hand, and relative surface area of the particles smaller than a definite equivalent diameter on the other hand.

The equivalent diameter-thickness ratio is about 20, close to Nadeau's (1987) ratio of 33 for illitic particles. The equivalent diameter-thickness relation was assumed to be linear, but it is probably not linear for the largest particles.

Polyphasic samples from the diagenetic environment. Lanson and Champion (1991) established the coexistence of two different authigenic I/S phases (plus a detrital micaceous phase) in these samples. The relative proportions of these different phases were determined from the relative intensities of related elementary peaks fitted on the experimental patterns. From this decomposition treatment, it was also possible to make preliminary assumptions about the illite content and the mean CSDS of both I/S phases. These preliminary assumptions allow us to determine the various parameters (composition, CSDS distribution, ordering type, and relative proportion of each elementary phase) faster and more accurately by trial-and-error simulation method. The best fits, shown on Figures 4a–c, were obtained assuming the calculated mixtures described below:

C1000: I/S (86% illite), R 1 maximum ordering, $3 \leq N \leq 16$ (triangular distribution): 60%.

I/S (94% illite), R 1 maximum ordering, 7 ≤ N ≤ 16 (triangular distribution): 34%.
Mica (100% illite), 15 ≤ N ≤ 85 (triangular distribution): 6%.

C1475: I/S (88% illite), R 1 maximum ordering, 3 ≤ N ≤ 16 (triangular distribution): 44%.
I/S (94% illite), R1 maximum ordering, 11 ≤ N ≤ 20 (triangular distribution): 30%.
Mica (100% illite), 15 ≤ N ≤ 85 (triangular distribution): 26%.

C2130: I/S (92% illite), R 1 maximum ordering, 7 ≤ N ≤ 16 (triangular distribution): 14%.
I/S (98% illite), R 1 maximum ordering, 11 ≤ N ≤ 20 (triangular distribution): 48%.
Mica (100% illite), 15 ≤ N ≤ 85 (triangular distribution): 38%.

Mixed-layer illite/smectite identification diagrams

The decomposition of experimental XRD profiles gives us the characteristics (i.e., position and FWHM) of the elementary peaks associated with the different clay phases present in the samples. The simulations allow one to follow the theoretical evolution of both position and FWHM of simulated peaks as a function of the initial parameters (CSDS, junction probabilities of different layers, and % smectite).

The structures of the end-members, junction probabilities, and CSDS for these calculations are given by Lanson (1990). Only the major band from 5°–10°2θ CuKα was considered. The subsidiary bands, related to the interference function oscillations (Reynolds, 1980, 1989) and not to a distinct phase, were ignored (Lanson, 1990; Lanson and Champion, 1991). On Figure 5, one can observe the FWHM variations as a function of peak position for mixed-layer illite/smectite hydrated with two interlayer water sheets (R = 1, maximum ordering). On this figure, one can note that the maximum FWHM is about 1.6°2θ CuKα. As described previously (Reynolds and Hower, 1970; Reynolds, 1980), the FWHMs measured on experimental spectra are greater than this value.

Lanson (1990) showed that the discrepancy in FWHM observed between simulated and experimental profiles cannot be induced by the presence of three-component mixed-layering (illite, smectite-1H_2O, smectite-2H_2O) or by the existence of partial ordering in the stacking sequence. The diagrams obtained by assuming either the hydration of some of the smectitic layers with only one interfoliar water sheet (three components: illite, smectite-1H_2O, smectite-2H_2O), and/or the existence of partial ordering in the stacking sequence are very similar to the one shown on Figure 5. Increased FWHM could also be obtained for simulated profiles by assuming lattice strain (Ergun, 1970; Reynolds, 1989). The peak broadening is then related to the displacements of the different atoms and layers about their nominal positions along the c* axis. Without a program available to calculate this, the effect of strain on peak width was not checked. Another phenomenon that could increase the simulated peaks FWHM is the occurrence of defects in the stacking sequence (Reynolds, 1989). However, this defect broadening effect is simply a particular form of the CSDS distribution.

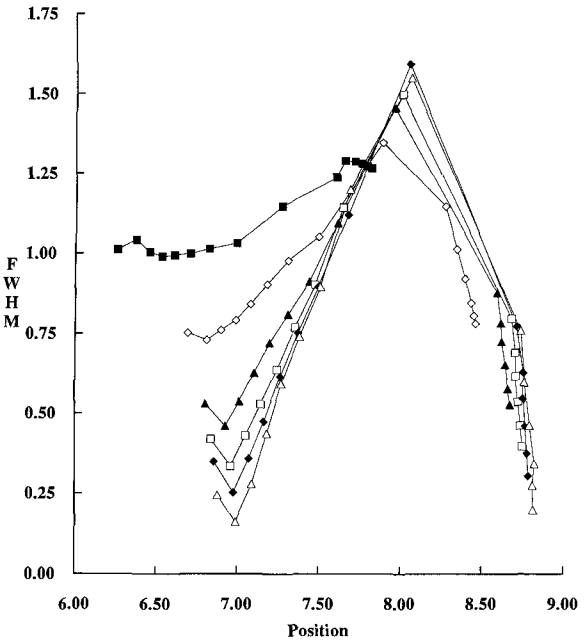

Figure 5. Identification diagrams for ordered (R = 1) mixed-layer illite/smectite. Position and width (FWHM) are given in °2θ CuKα. Illite/smectite (hydrated with two interfoliar water sheets), mixed-layer. Maximum ordering. The patterns represent CSDS distributions (solid squares: 2 ≤ N ≤ 5; open diamonds: 6 ≤ N ≤ 9; solid triangles: 11 ≤ N ≤ 14; open squares: 16 ≤ N ≤ 19; solid diamonds: 22 ≤ N ≤ 25; open triangles: 36 ≤ N ≤ 39). The compositions vary from 45–100% Illite (5% Ill steps from 45–90% Ill, and 2% Ill increments from 90–100% Ill).

The whole set of simulations (Lanson, 1990) encompasses most of the usual simulations (maximum ordering, and exclusive presence of smectite hydrated with two water layers). The set also shows the relative influence of CSDS, of smectite hydrated with one water layer, and of partial ordering in the stacking sequence. The diagrams in Lanson (1990) should allow one to identify I/S or illitic phases present in any natural sample. Unfortunately, the peak-width problems did not permit this identification.

Limitations and reproducibility of the decomposition method

Natural peak symmetry. The decomposition method was performed on a hydrothermal sample containing only one interstratified phase in order to check the resulting pattern for symmetry. The selected sample was from the hydrothermal series of samples studied

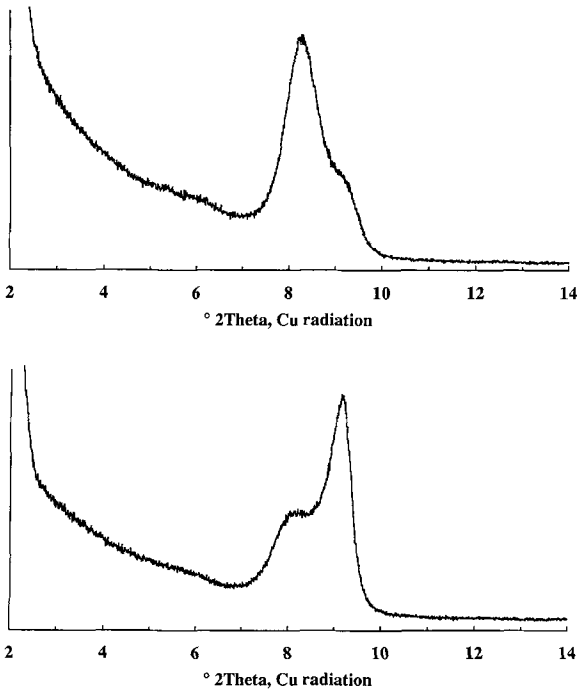

Figure 6. Sample WS7-115 (Inoue *et al.*, 1988). X-ray patterns; AD (top) and EG (bottom).

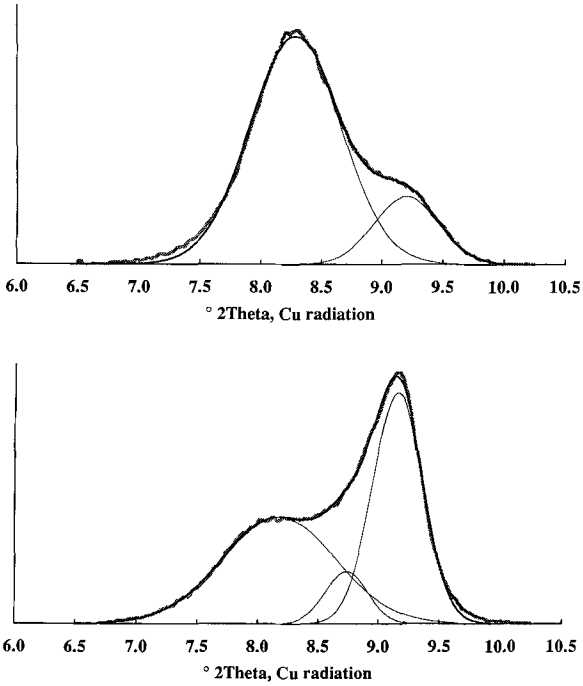

Figure 7. Decomposition of X-ray patterns, AD and EG (respectively, on top and bottom) from sample WS7-115.4 (15% Sm).

by Inoue *et al.* (1978, 1987, 1988), Inoue and Utada (1983), and Inoue (1986).

The AD and EG profiles of this sample (WS7-115.4) are shown on Figure 6. On the AD pattern one can note the apparent symmetry of the major peak at 8.3°2θ (10.65 Å) related to the interstratified phase, and the presence of a weak peak located around 9.3°2θ (9.5 Å). According to Mering's rule (Mering, 1949; Moore and Reynolds, 1989), this latter peak is also induced by the R $\geq$ 3 structure of this hydrothermal I/S (Inoue *et al.*, 1987). One can see that both of these peaks are symmetrical on the AD pattern (Figure 7). On the EG pattern decomposition, the interstratified structure also gives two peaks, one on each side of 10.00 Å, according to the simulations. Both of these peaks are symmetrical. However, it was necessary to introduce a weak additional peak in order to simulate accurately the shoulder between the two peaks. This weak peak also can be observed on simulated patterns; it is then induced by the interference function. Finally, despite the theoretical problems, the approximation of a mixed-layer I/S diffraction peak by a symmetric curve is realistic, even in the low-angle range.

Reproducibility. The influence of the various experimental procedures (running of the sample, preparation and selection of the sample) on the measurements of the parameters obtained with the numerical treatment of X-ray patterns was quantified by Lanson (1990). This author performed a series of tests: (1) repeated runs of the same slide under the same experimental conditions, (2) various runs of the same slide with different counting times, (3) runs of several slides prepared from the same suspension, (4) runs of several slides prepared from samples from the same outcrop, and (5) runs of several slides prepared from cored samples from the same stratigraphic level (on gamma-ray logs), in several wells from the same area (kilometer scale).

Lanson (1990) showed that the counting time has a small influence on the profile shape, except for 1 s counting times that are insufficient to give reproducible counting statistics. He also demonstrated that the standard deviations for all the series of tests define a single trend as a function of position and FWHM of fitted elementary peaks. This trend suggests that the standard deviation is induced mostly by the experimental equipment; that the calculated characteristics are representative of the sample studied; and that this sample is representative of the diagenetic evolution of its stratigraphic level in the studied area. Furthermore, the standard deviations on position and FWHM of an I/S peak (related to the illite content and the CSDS scatter of the associated phase) are larger when mean smectite content is high, than when mean CSDS is low.

Plotting the standard deviations on calculated positions (0.20°2θ when the position is 7.25°2θ, and 0.05°2θ when the position is around 8.80°2θ) in the identification diagrams, the error on estimated composition

(% illite) related to the experimental procedure is about ±2% Sm for illitic material, and ±3% Sm for less-illitic, ordered mixed-layer I/S.

Resolution of the method. To define the limits of the decomposition method, it was necessary to know its resolving power, i.e., its ability to separate the contributions of two populations with similar characteristics. Lanson (1990) showed that this decomposition method allows one to individualize the contributions of two interstratified phases with similar characteristics (differences of 0.3° and 0.2°2θ CuKα on position and FWHM, respectively, for the two most closely distinguishable peaks). It is even possible to distinguish peaks for which the difference in one of the peak characteristics is smaller if the contrast for the characteristics is larger. This is very frequently the case in the natural series studied (at least for the AD profiles).

This author also estimated that the error in the determination of XRD characteristics induced by the mixture of two phases is less than 2% illite for the kinds of mixtures that are analogous to those observed in a natural series. These observations are appropriate if the constituents of the mixture are in equal relative proportions. No test was done assuming variable relative proportions of the phases in order to observe the resulting mixture effect.

Influence of ethylene glycol saturation on true mica particles. To verify whether the shifts of the various elementary peaks could be due to an interparticle swelling effect, a ground muscovite (<2-μm particles as shown by TEM observations) slide was ethylene glycol-saturated. A comparison of the AD and EG profiles of this muscovite was performed using the decomposition method. The ethylene glycol saturation might demonstrate swelling of this fully micaceous phase if interparticle diffraction does occur.

We showed earlier that the asymmetry of this particular profile is related to the CSDS distribution, and that it is not an artifact of the experimental equipment, an artifact of the calculation method, an effect of grinding, or the result of interference function oscillations. Lanson (1990) established that the band characteristics do not vary after the EG saturation; the profile shape is the same for both AD and EG profiles. Consequently, if there is a shift in any elementary peak characteristic after EG saturation, this shift is actually related to the presence of expandable layers in the stacking sequence and not to interparticle diffraction effect, at least for particles with CSDS greater than ten layers.

Influence of cation exchange. Samples were not exchanged with a single cation (e.g., Sr) during slide preparation. Thus, one cannot know precisely the hydration state of smectitic layers, i.e., the number (one or two) of interfoliar water sheets if significant Na or K is present. The relative humidity was not controlled during the runs.

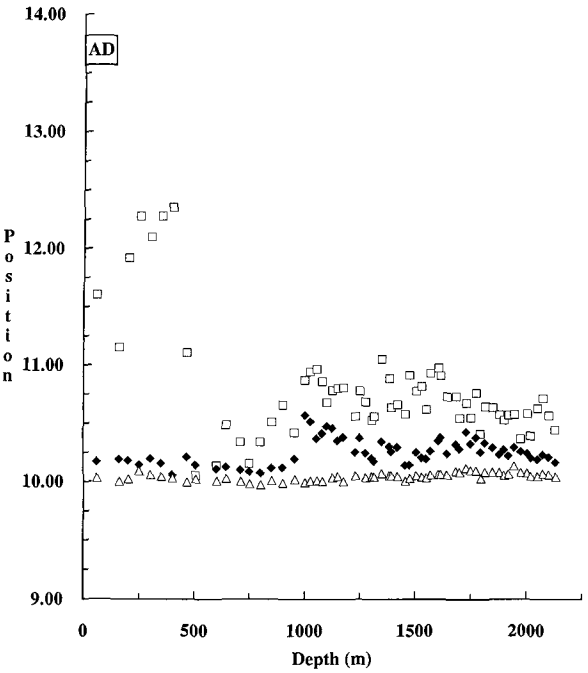

Figure 8. Evolution of position (Å) vs depth (meters) for Well C. The positions are obtained from decomposition of AD X-ray patterns. Patterns indicate the phases associated with the different elementary peaks: empty triangles: detrital mica (1st peak); solid diamonds: illite (2nd peak); empty squares: mixed-layer illite/smectite (ordered, 3rd peak).

Comparing the decomposition results from both natural and Sr-exchanged (the samples were put into suspension in 0.5 M $SrCl_2$ solution, and rinsed with distilled water to remove the excess $SrCl_2$) slides of six characteristic samples, Lanson (1990) showed that the difference in the characteristics of both samples was close to the standard deviation of the experimental procedure. Consequently, the phases related to these peaks can be identified with diagrams calculated assuming two interfoliar water (or EG) sheets.

Application to sedimentary series

On TEM micrographs of our samples, Lanson and Champion (1991) identified lath-shaped particles and hexagonal plates, as well as detrital phases easily distinguishable due to their greater contrast. Analyzing individual particles by EDS methods, they demonstrated that the two particle types are different chemically. The chemical compositions of both types of particles occur in the non-mica domain; the chemical composition of laths varies as a function of depth, indicating a change in their smectite content. They showed that the samples contain two authigenic phases (one I/S mixed-layer phase, and an illitic phase), a detrital micaceous phase, and occasionally chlorite and/

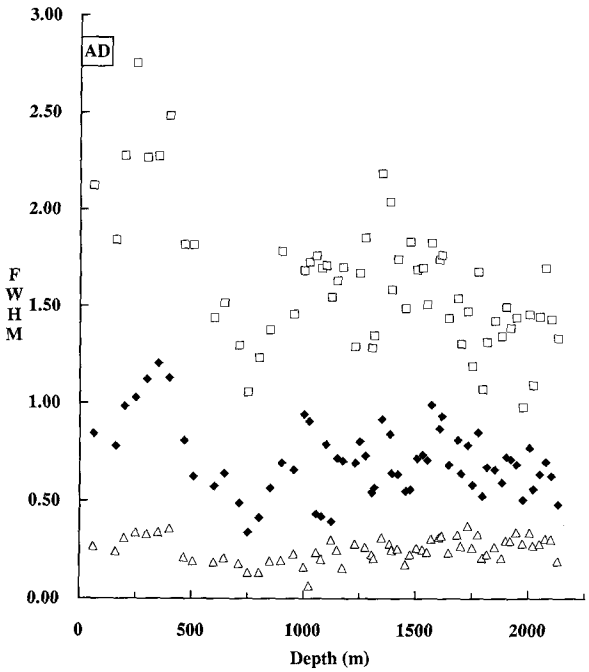

Figure 9. Evolution of full width at half maximum (°2θ CuKα) vs depth (meters) for Well C. The widths are obtained from decomposition of AD X-ray patterns. Patterns as Figure 8.

or kaolinite. The complex diffraction band from 4°–10°2θ CuKα should include the representative peaks of these phases (I/S, illite, mica ± chlorite). Except for the chlorite peak, all the decompositions performed on AD profiles required three elementary peaks to obtain a good fit (Lanson and Champion, 1991; Figure 2).

The sharper peak closer to 10 Å is called "1st peak." The "3rd peak" is found at the lowest 2-θ angle and its FWHM is the greatest. The "2nd peak" has an intermediate position and FWHM. These "peaks" are associated with detrital mica, an interstratified I/S phase, and "illite", respectively. For the more expandable samples, the EG profiles were decomposed into four elementary peaks (Lanson and Champion, 1991, Figure 3a; Figures 10, 11). When the I/S expandability decreases to a certain value (corresponding to about 1400 meters depth in the borehole), the resolving power of the decomposition method is insufficient to distinguish the 2nd "illitic" peak and the third doublet component located at higher angles. Consequently, the decomposition of such EG profiles was performed with only three elementary peaks (Lanson and Champion, 1991, Figure 3b: Figures 10, 11), one of the peaks representing two different phases (illite + I/S).

In Figures 8–11, one can note the great consistency of the results, except for the 450 to 950-meter depth range. In this range, the evolution of both position and FWHM of the different elementary peaks, continuous in the ranges on both sides of this particular level, show a hiatus. The corrensite occurrence in this particular stratigraphic sequence (from Keuper to Muschelkalk) is characteristic of deposits found in confined environment (Velde, 1985). The occurrence of this phase also implies chemical conditions (especially for Fe and Mg) very different from the conditions observed at the other stratigraphic levels. It seems that the observed mineralogical differences are related to these singular depositional conditions. The following discussion will be based on observations that ignore this interval.

On both AD and EG profiles, the first peak characteristics remain constant with depth (empty triangles on Figures 8–11). The position and FWHM, respectively, scatter from 10.00 to 10.10 Å, and from 0.15° to 0.35°2θ CuKα. These characteristics are not influenced by EG saturation. One can deduce that the phase associated with this peak does not contain any swelling layers. Furthermore, this well-crystallized phase is present from the surface down, and does not show any evolution. It was identified as a detrital micaceous phase.

The characteristics of the second peak (solid diamonds on Figures 8–11) are also constant with depth: position and FWHM, respectively, scatter from 10.15 to 10.50 Å, and from 0.50° to 1.20°2θ. The FWHM remains constant after EG saturation; the observed shift in peak position after glycolation is due to the impossibility of distinguishing the illite and I/S phases. On

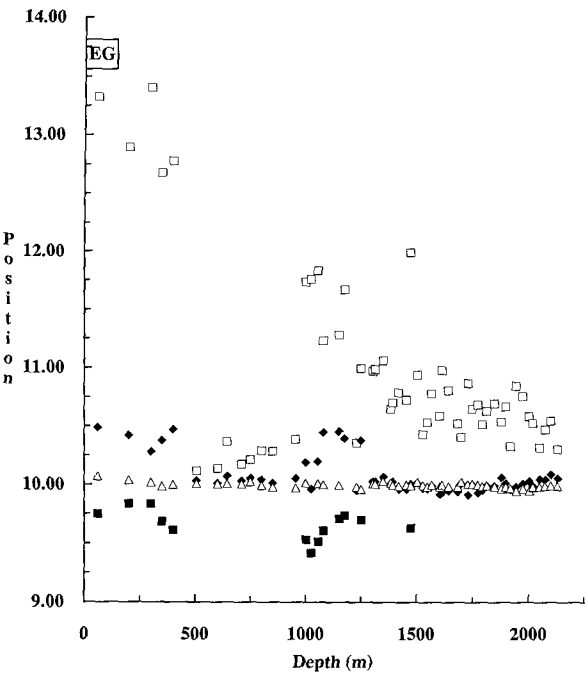

Figure 10. Evolution of position (Å) vs depth (meters) for Well C. The positions are obtained from decomposition of EG X-ray patterns. The patterns indicate the phases associated with the different elementary peaks: empty triangles: detrital mica; solid diamonds: illite; empty and solid squares: mixed-layer illite/smectite (ordered).

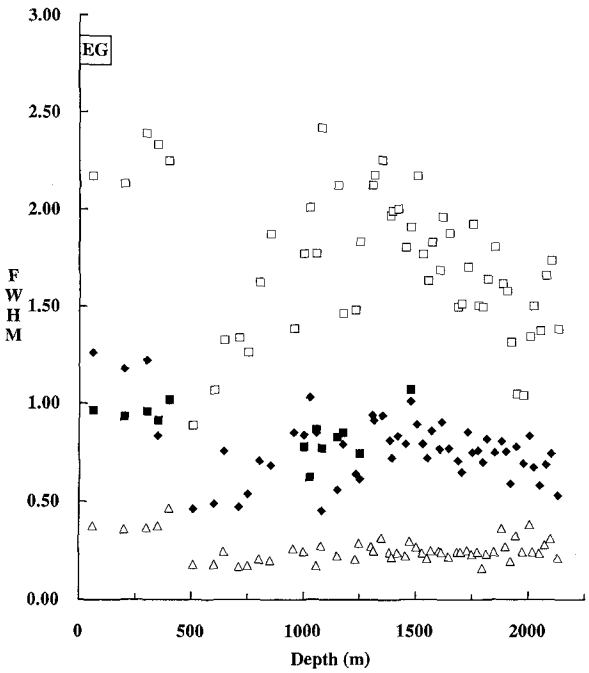

Figure 11. Evolution of full width at half maximum (°2θ CuKα) vs depth (meters) for Well C. The widths are obtained from decomposition of EG X-ray patterns. Patterns as Figure 10.

Figures 9 and 11, one can note that the FWHM of this second peak decreases slightly with depth. This decrease could be related to an increase in illite content (very close to 100% illite) and/or to an increase in mean CSDS.

Finally, the third peak exhibits a clear trend on both position and FWHM on AD profiles. The position decreases from 12.25 Å (surface) to 10.50 Å (2130 meter-deep sample), while the FWHM decreases from about 2.50° to 1.25°2θ CuKα. Even if the elementary peaks fitted to the experimental patterns are too wide when compared to the simulated ones, it is likely that the trends defined by the simulations are correct (position closer to 10 Å as the I/S becomes more illitic, and decreasing FWHM as the CSDS gets larger). By analogy, one can assume that the simultaneous evolution of position and FWHM with depth is associated with a decrease in the smectite content and an increase in mean CSDS. These hypotheses are supported by the observations performed by Lanson and Champion (1991) on I/S mixed-layer, lath-shaped particles, which are associated with the third peak. They demonstrated the simultaneous evolution of the chemical composition of these particles toward the illite composition (and thus an increase in the illite content of these particles) and of the *ab*-surface area of these particles (and thus probably of their thickness). The same trends are shown on EG profiles.

SUMMARY AND CONCLUSIONS

The theoretical fits shown on Figures 1 and 4 are close to the experimental profiles. This crystallographic method allows an accurate identification of the various phases existing in a sample, even in a complex case such as the diagenetic environment. However, one must remember that it is necessary to determine physico-chemical characteristics separately for each phase in order to use this method (Drits and Sakharov, 1976; Tchoubar *et al.*, 1990). For a pure interstratified sample, it is very time-consuming to determine the chemical composition, the relative proportions of each component, the junction probabilities, and the CSDS distribution. Thus, it is unlikely that this method will be used routinely to characterize precisely the different mixed-layer phases present in a sedimentary sample.

The decomposition method described allows one to follow accurately the diagenetic evolution of clay minerals. Because the method is simple and not especially time-consuming it can be performed on a great number of samples. The estimated error on smectite content induced by the mixing effect ($\leq$2% Sm) and the experimental procedure ($\leq$3% Sm) is low. At present, it is not possible to determine the exact nature (especially illite content and CSDS), because of the differences observed between the characteristics of natural minerals and of simulated profiles. By looking at higher-order peaks, it is possible to eliminate these differences (Lanson, in preparation). However, this does not eliminate the peak-width problem on the band considered in this paper. Thus, it is necessary to introduce new simulation hypotheses such as thermal vibration of atoms, which is equivalent to considering a population of elementary layers that have basal distances that vary about a mean value. The introduction of faults in the stacking sequence could also be a parameter that induces an important peak broadening (Reynolds, 1989). These faults can either induce a different CSDS distribution (Reynolds, 1985), or be induced by the presence of incomplete T–O–T layers (e.g., T–O layers) and/or gibbsite-like layers in the stacking sequence.

The present method is very powerful for following diagenetic trends. It can also be used to make detailed simulations much easier by obtaining preliminary results on the nature of the different phases, and their relative proportions. However, one must remember the initial warnings concerning this decomposition method, and consequently try to check the results obtained from this X-ray profile shape numerical treatment by using other methods of analysis (Lanson and Champion 1991).

ACKNOWLEDGMENTS

We thank the Institut Français du Pétrole and Gaz de France for providing the samples. B.L. acknowledges financial support from the Institut Français du

Pétrole. The manuscript benefited from reviews by D. D. Eberl, B. Velde and R. C. Reynolds, Jr.

REFERENCES

Ben Hadj-Amara, A., Besson, G., and Tchoubar, C. (1987) Caractéristiques structurales d'une smectite en fonction des relations d'ordre-désordre dans la distribution des charges életriques: *Clay Miner.* **22,** 305–318.

Besson, G. (1980) Structures des smectites dioctaédriques. Paramètres conditionnant les fautes d'empilement des feuillets: Thesis, University of Orléans, France, 153 pp.

Boles, J. R. and Franks, G. S. (1979) Clay diagenesis in Wilcox sandstones of Southwest Texas: Implications of smectite diagenesis on sandstone cementation: *J. Sed. Petrol.* **49,** 55–70.

Burst, J. F. (1969) Diagenesis of Gulf Coast clayey sediments and its possible relation to petroleum migration: *Amer. Assoc. Petrol. Geol. Bull.* **53,** 73–93.

Drits, V. A. and Sakharov, B. A. (1976) *X-ray Structure Analysis of Mixed-layer Minerals.* Dokl. Akad. Nauk SSSR, Moscow, 256 pp. (in Russian).

Ergun, S. (1970) X-ray scattering by very defective lattices: *Physical Review* **B-131,** 3371–3380.

Freed, R. L. and Peacor, D. R. (1989) Variability in temperature of the smectite/illite reaction in Gulf Coast sediments: *Clay Miner.* **24,** 171–180.

Glasmann, J. R., Larter, S., Briedis, N. A., and Lundegard, P. D. (1989) Shale diagenesis in the Bergen High area, North Sea: *Clays & Clay Minerals* **37,** 97–112.

Hendricks, S. D. and Teller, E. (1942) X-ray interference in partially ordered layer lattices: *J. Chem. Phys.* **10,** 147–167.

Howard, S. A. and Preston, K. D. (1989) Profile fitting of powder diffraction patterns: in *Modern Powder Diffraction, Reviews in Mineralogy,* **20,** D. L. Bish and J. E. Post, eds., Mineral. Soc. of Amer., Washington, D.C., 217–275.

Hower, J., Eslinger, E. V., Hower, M. E., and Perry, E. A., Jr. (1976) Mechanism of burial metamorphism of argillaceous sediment: 1. Mineralogical and chemical evidence: *Geol. Soc. Amer. Bull.* **87,** 725–737.

Inoue, A. (1986) Morphological change in a continuous smectite-to-illite conversion series by scanning and transmission electron microscopies: *J. Coll. Arts & Sci., Chiba Univ.* **B-19,** 23–33.

Inoue, A., Kohyama, N., Kitagawa, R., and Watanabe, T. (1987) Chemical and morphological evidence for the conversion of smectite to illite: *Clays & Clay Minerals* **35,** 111–120.

Inoue, A., Minato, H., and Utada, M. (1978) Mineralogical properties and occurrence of illite/montmorillonite mixed layer minerals formed from Miocene volcanic glass in Waga-Omono district: *Clay Sci.* **5,** 123–136.

Inoue, A. and Utada, M. (1983) Further investigations of a conversion series of dioctahedral mica/smectites in the Shinzan hydrothermal alteration area, northeast Japan: *Clays & Clay Minerals* **31,** 401–412.

Inoue, A., Velde, B., Meunier, A., and Touchard, G. (1988) Mechanism of illite formation during smectite-to-illite conversion in a hydrothermal system: *Amer. Mineral.* **73,** 1325–1334.

Inoue, A., Watanabe, T., Kohyama, N., and Brusewitz, A. M. (1990) Characterization of illitization of smectite in bentonite beds at Kinnekulle, Sweden: *Clays & Clay Minerals* **38,** 241–249.

Jennings, S. and Thompson, G. R. (1986) Diagenesis of Plio-Pleistocene sediments of the Colorado river delta, southern California: *J. Sed. Petrol.* **56,** 89–98.

Lahann, R. W. (1980) Smectite diagenesis and sandstone cement: The effect of reaction temperature: *J. Sed. Petrol.* **50,** 755–760.

Lanson, B. (1990) Mise en évidence des mécanismes de transformation des interstratifiés illite/smectite au cours de la diagenèse: Ph.D. thesis, Univ. Paris, France, 366 pp.

Lanson, B. and Champion, D. (1991) The I/S to illite reaction in the late stage diagenesis: *Amer. J. Sci.* **291,** 473–506.

Méring, J. (1949) L'interférence des rayons-X dans les systèmes à stratification désordonnée: *Acta Crystallogr.* **2,** 371–377.

Moore, D. M. and Reynolds, R. C. (1989) *X-ray Diffraction and the Identification and Analysis of Clay Minerals:* Oxford Univ. Press, 243–246.

Nadeau, P. H. (1985) The physical dimensions of fundamental clay particles: *Clay Miner.* **20,** 499–514.

Nadeau, P. H. (1987) Relationships between the mean area, volume and thickness for dispersed particles of kaolinites and micaceous clays and their application to surface area and ion exchange properties: *Clay Miner.* **22,** 351–356.

Nadeau, P. H., Tait, W. J., McHardy, W. J., and Wilson, M. J. (1984a) Interstratified XRD characteristics of physical mixtures of elementary clay particles: *Clay Miner.* **19,** 67–76.

Nadeau, P. H., Wilson, M. J., McHardy, W. J., and Tait, J. M. (1984b) Interparticle diffraction concept for interstratified clays: *Clay Miner.* **19,** 757–769.

Nelder, J. A. and Mead, R. (1965) A simplex method for function minimization: *Computer Journal* **7,** 308–313.

Perry, E. A., Jr. and Hower, J. (1970) Burial diagenesis in Gulf Coast pelitic sediments: *Clays & Clay Minerals* **18,** 165–177.

Press, W. H., Flannery, B. P., Teukolsky, S. A., and Vetterling, W. T. (1986) *Numerical Recipes. The Art of Scientific Computing:* Cambridge Univ. Press, 818 pp.

Reynolds, R. C. (1980) Interstratified clay minerals: in *Crystal Structures of Clay Minerals and their X-ray Identification,* G. W. Brindley and G. Brown, eds., Mineral. Soc., London, 249–359.

Reynolds, R. C. (1985) *NEWMOD© a computer program for the calculation of one-dimensional patterns of mixed-layered clays:* R. C. Reynolds, 8 Brook Rd., Hanover, New Hampshire.

Reynolds, R. C. (1986) The Lorentz-polarization factor and preferred orientation in oriented clay aggregates: *Clays & Clay Minerals,* **34,** 359–367.

Reynolds, R. C. (1989) Diffraction by small and disordered crystals: in *Modern Powder Diffraction, Reviews in Mineralogy,* **20,** D. L. Bish and J. E. Post, eds., Mineral. Soc. of Amer., Washington, D.C., 145–181.

Reynolds, R. C. and Hower, J. (1970) The nature of interlayering in mixed-layer illite-montmorillonites: *Clays & Clay Minerals* **18,** 25–36.

Sakharov, B. A. and Drits, V. A. (1973) Mixed-layer kaolinite-montmorillonite: A comparison of observed and calculated diffraction patterns: *Clays & Clay Minerals* **21,** 15–17.

Środoń, J. (1979) Correlation between coal and clay diagenesis in the Carboniferous of the upper Silesian coal basin: in *Proc. Int. Clay Conf., Oxford, 1978,* M. M. Mortland and V. C. Farmer, eds., Elsevier, Amsterdam, 251–260.

Środoń, J. (1980) Precise identification of illite/smectite interstratifications by X-ray powder diffraction: *Clays & Clay Minerals* **28,** 401–411.

Środoń, J. (1981) X-Ray identification of randomly interstratified illite-smectite in mixtures with discrete illite: *Clay Miner.* **16,** 297–304.

Środoń, J. (1984a) Mixed-layer illite-smectite in low-tem-

perature diagenesis: Data from the Miocene of the Carpathian foredeep: *Clay Miner.* **19,** 205–215.

Środoń, J. (1984b) X-ray powder diffraction of illitic materials: *Clays & Clay Minerals* **32,** 337–349.

Środoń, J. and Eberl, D. D. (1984) Illite: in *Micas, Reviews in Mineralogy* **13,** S. W. Bailey, ed., Mineral. Soc. of Amer., Washington, D.C., 495–544.

Tchoubar, C., Drits, V. A., Besson, G., Bookin, A. S., Rousseaux, F., Sakharov, B. A., and Tchoubar, D. (1990) *X-ray Diffraction by Disordered Lamellar Structures. Theory and Applications to Microdivided Silicates and Carbons:* Springer-Verlag, Berlin.

Velde, B. (1985) Clays Minerals: A physico-chemical explanation of their occurrence: *Developments in Sedimentology* **40,** Elsevier, Amsterdam, 427 pp.

Velde, B. and Espitalié, J. (1989) Comparison of kerogen maturation and illite/smectite composition in diagenesis: *J. Petrol. Geol.* **12,** 103–110.

Velde, B., Suzuki, T., and Nicot, E. (1986) Pressure-temperature-composition of illite/smectite mixed-layer minerals: Niger delta mudstones and other examples: *Clays & Clay Minerals* **34,** 435–441.

Watanabe, T. (1981) Identification of illite/montmorillonite interstratification by X-ray powder diffraction: *J. Miner. Soc. Jap. Spec. Issue* **15,** 32–41 (in Japanese).

Watanabe, T. (1988) The structural model of illite/smectite interstratified minerals and the diagram for their identification: *Clay Sci.* **7,** 97–114.

(Received 6 June 1991; accepted 5 November 1991; Ms. 2108)